



Rockfall susceptibility along Pasang Lhamu and Galchhi-Rasuwadadi highways, Rasuwa, Central Nepal

Badal Pokharel¹ · Samsung Lim^{1,2} · Tara Nidhi Bhattarai³ · Massimiliano Alvioli⁴

Received: 27 October 2022 / Accepted: 14 March 2023
© The Author(s) 2023

Abstract

The road network in Central Nepal suffered blockades and damage from numerous landslides and rockfalls due to the earthquake sequence in Gorkha, Nepal, in 2015. Additionally, frequent rainstorms in the area contributed to the recurrence of rockfalls and other types of landslides, hindering road infrastructure development and environmental management. Despite the several existing regional and local studies on landslide susceptibility in the area, rockfall-specific analysis is still lacking. In this paper, we assessed rockfall susceptibility in the sections of the Pasang Lhamu highway and the Galchhi-Rasuwadadi highway in the Rasuwa district using a physically based model. We generated three-dimensional rockfall trajectories along the roads and used them to infer the rockfall susceptibility of the area. We selected potential locations for the initiation of rockfalls based on the optimization of the gridded slope angle, relief, and terrain ruggedness, validated the source map using statistical parameters, and compared them with a field-mapped rockfall source inventory. As a result, we identified which road sections in Ramche, Dandagaun, and Syaprubesi are highly susceptible to rockfalls. We published the field-based inventory of rockfall sources and segment-wise rockfall susceptibility of highways, where a rockfall susceptibility index of 5 indicated very high susceptibility and 1 very low susceptibility. Such findings and maps are helpful for researchers, land planners, developers, government bodies working on disaster risk reduction, and policymakers to design a preliminary framework for rockfall mitigation and sustainable roads.

Keywords Gorkha earthquake · Rockfalls · Rockfall susceptibility map · Himalayas · Risk reduction

Introduction

Rockfalls are frequent hazards on steep mountain slopes, often affecting road networks, causing casualties and significant economic loss (Guzzetti 2000; Guzzetti et al. 2004; Chen et al. 2009; Cignetti et al. 2021). The Himalayan belt is a seismically active region and comprises many unstable slopes likely to suffer from earthquake-triggered landslides,

including rockfalls (Vishal et al. 2015; Vishal et al. 2017; Pradhan et al. 2015). Apart from the seismicity, other factors responsible for rockfalls are high precipitation, complex topography, and anthropogenic activities, including road cuts.

The Nepal Himalayas region is an example in the Himalayan belt, where rockfall events occur yearly. For instance, the rockfalls of the Siddhababa region along the Siddhartha Highway and the Jogimara region along the Prithvi highway greatly affected lives and properties. Local newspapers reported that rock crushing on road traffic caused numerous human casualties in these regions. Moreover, the disastrous earthquake of Mw 7.8 in Gorkha, Nepal, in 2015 triggered numerous landslides, including rockfalls along the central Nepal Himalayan belt that severely affected road networks (Collins and Jibson 2015; Martha et al. 2017). The frequency of rockfalls increased after the Gorkha earthquake event, specifically along the Araniko Highway in central Nepal, affecting livelihoods and infrastructure, as Regmi et al. (2016a) reported; it also pointed out that most rockfalls were topples, and some

✉ Badal Pokharel
b.pokharel@unsw.edu.au

¹ School of Civil and Environmental Engineering, University of New South Wales, Sydney, Australia
² Biosecurity Program, Kirby Institute, University of New South Wales, Sydney, Australia
³ Department of Geology, Tri-Chandra Multiple Campus, Tribhuvan University, Kathmandu, Nepal
⁴ Istituto Di Ricerca Per La Protezione Idrogeologica, Consiglio Nazionale Delle Ricerche, Via Madonna Alta 126, 06128 Perugia, Italy

others were wedge and plane failures. Physical impacts created by such phenomena affected not only people and properties but also the environment, natural resources, and landscape patterns (Lin et al. 2006).

The Pasang Lhamu highway (PLH), which connects Kathmandu, Nepal's capital city, with Tibet of China, was one of the worst affected highways, apart from the Arniko Highway, due to coseismic landslides related to the earthquake (Xu et al. 2017). Several landslides triggered by Gorkha earthquake-related aftershocks also affected the Galchhi-Rasuwadhi highway (GRH), one of the busiest trade road networks that joined Galchi and Rasuwadhi. Rockfalls that occurred during and after the earthquake obstructed these highways and major roads, impeding supplies of basic goods (e.g., food and medicine), and trade. To date, these highways strive to recover from the damages created by the Gorkha earthquake. However, frequent rockfall incidents have made the recovery process difficult.

Rockfall susceptibility mapping is crucial along these highways to mitigate the impact of future disruptive events as a prior step to obtaining rockfall hazard and risk maps. This will help the authorities to articulate strategies to prioritize susceptible road sections, aiming to conduct a detailed investigation to mitigate rockfalls, design preventive measures, and help in land use planning. Few research has been conducted to assess the rockfall susceptibility along these highways (Lacroix 2016; Pokharel and Thapa 2019; Pokharel et al. 2021a; Amatya et al. 2021).

Previous studies highlighted the importance of assessing natural hazard susceptibility to indicate sections of road networks that would require attention in ensuring roadside safety, proper land use planning, and environmental management (Guillard and Zezere 2012; Karlsson et al. 2017). To do so, one needs to ensure that the natural hazard inventories (e.g., landslides, floods, ground subsidence) are representative and of high quality because, ultimately, this will determine the effectiveness of the susceptibility maps. Guzzetti et al. (2012), Pokharel et al. (2021b), and Loche et al. (2022) demonstrated how the quality and representativeness of landslide inventories affect the corresponding landslide susceptibility maps.

The dependence of landslide susceptibility assessment on general-purpose or uncategorized inventories (i.e., inventories in which the types of landslides are not distinguished) might be less effective due to the differences in the nature, causes, and triggering mechanisms of different landslide types. Therefore, it is crucial to use a landslide-specific inventory (e.g., rockfall inventory, debris flow inventory) for a reliable landslide susceptibility map. Past studies in this area mostly rely upon landslide inventories and are less relevant to rockfall susceptibility research. Therefore, this work aims to assess the rockfall susceptibility along the PLH

and the GRH using specific rockfall inventories mapped in the field, in conjunction with a quantitative model.

The primary step to assess rockfall susceptibility is the study of the rock discontinuities, including fractures and joints, rock mass orientation, and possible detachment areas. The approaches researchers adopt to assess susceptibility depend on the study's objective. For example, Antoniou and Lekkas (2010) evaluated rockfall susceptibility based on geology, geomorphology, and rockfall maximum runout of the blocks by applying an empirical model. Toševskito et al. (2021) prepared a talus inventory of the study area and used a combination of the seed-cell concept and statistical method to prepare a rockfall susceptibility map. In this article, we aim to include only those rock masses that ballistic dynamics can describe, such as blocks that fall under the action of gravity and coercion of geological and geomorphological factors.

To generate a rockfall susceptibility map (RSM), we used a physically based model called STONE (Guzzetti et al. 2002). STONE describes individual rock blocks starting from user-defined source locations and following independent trajectories (Alvioli et al. 2021, 2022c) under the sole action of gravity. This is very relevant to our study area, and the Central Nepal Himalayan belt, where most rock formations exposed on a steep cliff in the Lesser Himalayan and the Higher Himalayan Zones have crosscut joints that give rise to big boulders in case of a failure. STONE calculates a user-defined number of trajectories, which is an advantage for researchers working in the peculiar topography of the Rasuwa District, where surveys are time-consuming and difficult. Analysis of the trajectory count obtained from STONE and corresponding RSMs can help prioritize the assessment of the highly susceptible rockfall sites in the area.

To this end, we (i) mapped rockfall sources along PLH and GRH by conducting field investigation and satellite imagery analyses, (ii) applied the data-driven method (Alvioli et al. 2021, 2022b, 2023) to single out potential rockfall source areas, (iii) run STONE and obtained a raster map with trajectory count, to prepare an RSM, and (iv) compared with field data. We publish the field-based inventory of rockfall sources (Fig. 4) with this work as supplementary material. Results provide insight into rockfall susceptibility along the road network, which is helpful for rockfall hazard assessment and could be useful in land use planning (Cignetti et al. 2021), sustainable road design, and environmental management (Guzzetti et al 2004).

This work is organized as follows. The “study area” section describes the study area. The “Data and methodology” section gives context on the data available and prepared for this study and the methodology adopted in this work. The “Results” section describes the results, the “Discussions” section presents discussions, and the “Conclusions” section draws conclusions.

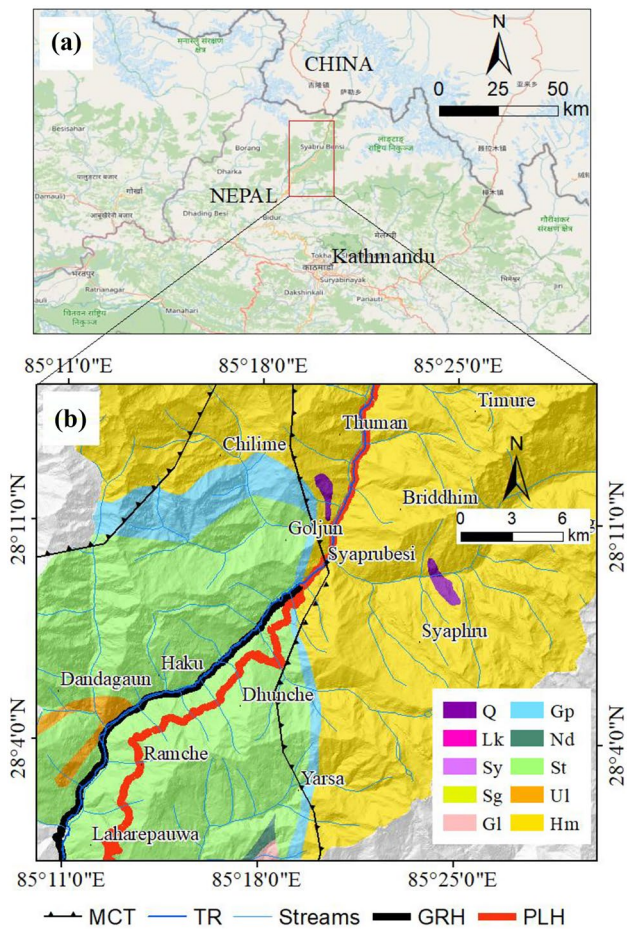
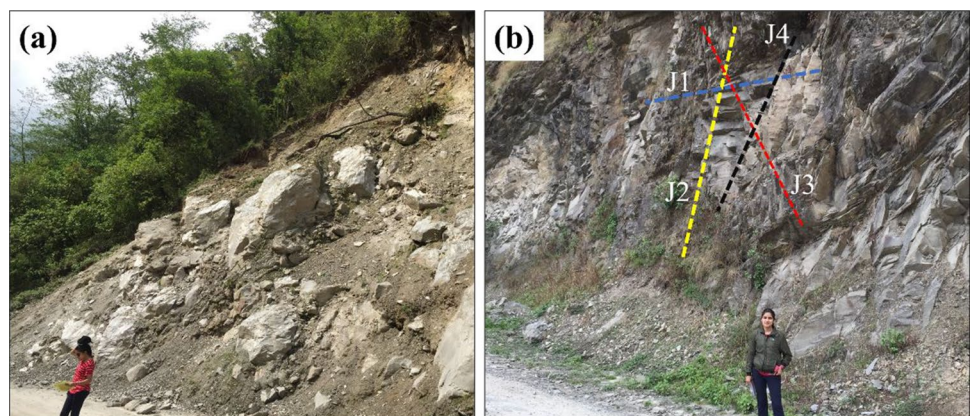


Fig. 1 a Map showing the geographical location of the study area; **b** geological map, modified after Stocklin (1980) and Department of Mines and Geology (DMG) (2011). Q, Recent deposits; Lk, Lkharpata formation; Sy, Syngja formation; Sg, Sangram formation; Gl, Galyang formation; Gp, Ghan Pokhara formation; Nd, Naudanda formation; St, Seti formation; Ul, Ulleri formation; Hm, Himal Group; MCT, Main Central Thrust; TR, Trisuli River; GRH, Galchhi-Rasuwa Highway; PLH, Pasang Lhamu Highway. The relevant infrastructure is also shown in **b**

Fig. 2 a High-moderately weathered slope along PLH at Dhunche, Rasuwa. **b** Example of a slope with four sets of joints represented by four colors (J1: blue, J2: yellow, J3: red, and J4: black). The slope is comprised of quartzite and lies along PLH at Dhunche, Rasuwa



Study area

The study area lies in the Rasuwa district in Central Nepal, one of the worst affected districts by the Gorkha earthquake in 2015 (Regmi et al. 2016b; Pokharel and Thapa 2019; Pokharel et al. 2021b). We investigated rockfall occurrences in the region from Laharepauwa to Goljun in an approximately 30 km section of PLH and GRH, shown in Fig. 1. The most affected villages by the earthquake-induced landslides, including rockfalls, are Ramche, Dandagaun, and Syaprubesi (Pokharel and Thapa 2019). Some of the landslides damaged and blocked the roads hindering transport. Rockfall events not only obstructed roads but also affected hydropower plants and settlements (Bhattarai and Dhital 2021).

Galchhi-Rasuwa highway runs parallel cutting the Trisuli river (TR, in Fig. 1) terrace, whereas PLH lies on the slope, at a much higher altitude than GRH. Altitude ranges from 405 to 7191 m (cf. the “Field mapping and preparation of data” section). Geologically, the area encompasses the Main Central Thrust (MCT, in Fig. 1), a major thrust fault system in the Nepal Himalayas, which separates the Lesser Himalayan metasediments from the Higher Himalayan Crystalline. The study site is comprised of ten geological units that mainly consist of dolomites, limestones, phyllite, schists, quartzite, and other metasedimentary rocks.

The potential rock blocks are mainly composed of phyllites, schists, and quartzites. An engineering geological investigation revealed that the weathering degree of the rocks along highways ranges from low to high in some places and moderate to high in some areas (Fig. 2a). The exposed rocks comprise at least three sets of joints (Fig. 2b). The region has steep high cliffs, and the intersection of joints is such that they are likely to form large rock blocks in case of failure. Such a condition of failure is prevalent in most of the steep slopes in the Rasuwa district (Bhattarai and Dhital 2021).

The climatic condition of the study area ranges from temperate in the south to polar tundra climate in the north. Maximum precipitation of approximately 880 mm occurring the summer monsoon months of July and August whereas November and December months receive minimum precipitation of 20 mm (Dawadi et al. 2022). Slope weathering is accelerated during monsoon season, commonly resulting in rock detachment, followed by rockslides and falls.

Due to the lack of long-term precipitation data and a small number of local rainfall stations, we did not include the effect of precipitation as a trigger mechanism in our study. In addition, other triggering factors such as seismicity, freezing-thaw cycles, and identification of detachment areas by failure mechanisms due to discontinuities in the rock slope are out of the scope of our study. Owing to the geology, geomorphology, and climatic conditions of this region, rockfalls are expected to be frequent, causing fatalities and infrastructure damage along these highways in the Rasuwa district.

Data and methodology

We conducted our study in the following steps: (i) field mapping and data preparation; (ii) selection of potential source area based on the slope, relief, and vector ruggedness measure (VRM); (iii) simulation of rockfall trajectories with STONE; and (iv) comparison and validation of results with field data. The flowchart in Fig. 3 illustrates the overall methodology of the study.

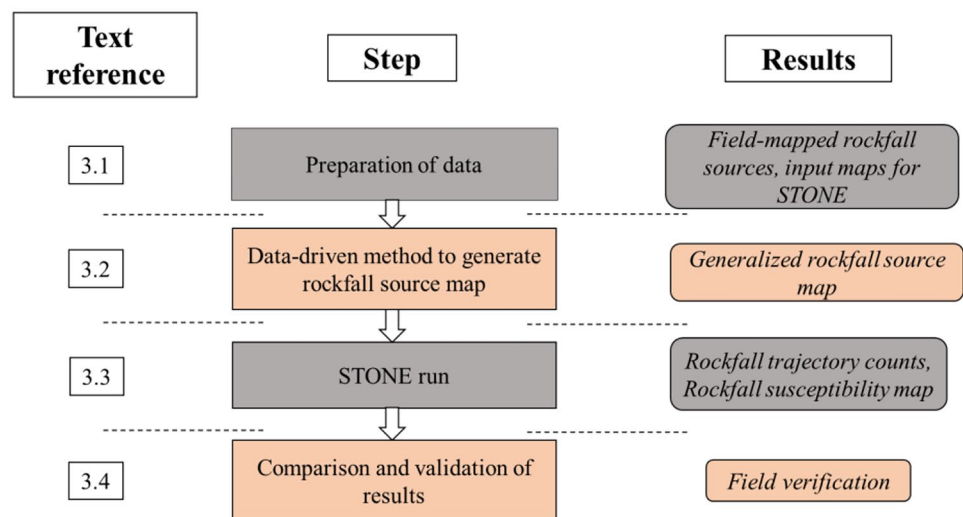
Field mapping and preparation of data

Our work required (i) a digital elevation model (DEM), (ii) rockfall source inventory, (iii) slope units covering the

highway and their surroundings, and (iv) a lithological map to infer numerical input parameters (dynamic friction, normal restitution, and tangential restitution) for STONE. In the following, we provide a piece of short information on each dataset.

- We used 12.5 m resolution ALOS DEM covering an area of 10,526.4 sq. km ($27^{\circ}51'12.6''$ N to $28^{\circ}14'44.12''$ N and $85^{\circ}5'7.08''$ E to $85^{\circ}24'10.44''$ E), freely available on the Alaska Satellite Facility Distributed Active Archive Centre (<https://vertex.daac.asf.alaska.edu>).
- We used slope units (SU), i.e., polygonal mapping units bounded by drainage and divide lines, similarly to Alvioli et al. (2021, 2022c) and Loche (2022), who also used slope units to prepare RSMs. Compared to the grid cell, SUs are more appropriate for studying landslides because of their strong correlation with topography and geomorphology (Alvioli et al. 2016, 2020; Jacobs et al. 2020; Domènech et al. 2020). Additionally, in our study, the main advantage is that rockfall trajectories originating in a specific SU are likely to stay bounded within the same SU (Alvioli et al. 2021). Slope units for the study area were published by Alvioli et al. (2022a). We surveyed 639 slope units in the field to prepare the rockfall inventory.
- We mapped 243 polygons corresponding to rockfall sources related to the Gorkha earthquake event between April 2015 and December 2016 (Fig. 4).
- Each source location was identified during our field survey (Fig. 5). We transferred the corresponding sources in GIS, cross-referencing the location with available Google Earth™ images and local reports. We only considered the rockfall sources that would likely give rise to compatibility with ballistic dynamics, which can be described by STONE (Guzzetti et al. 2002; Alvioli et al. 2021). The

Fig. 3 Illustration of the methodology adopted in the study. Text references correspond to the numbering of sections



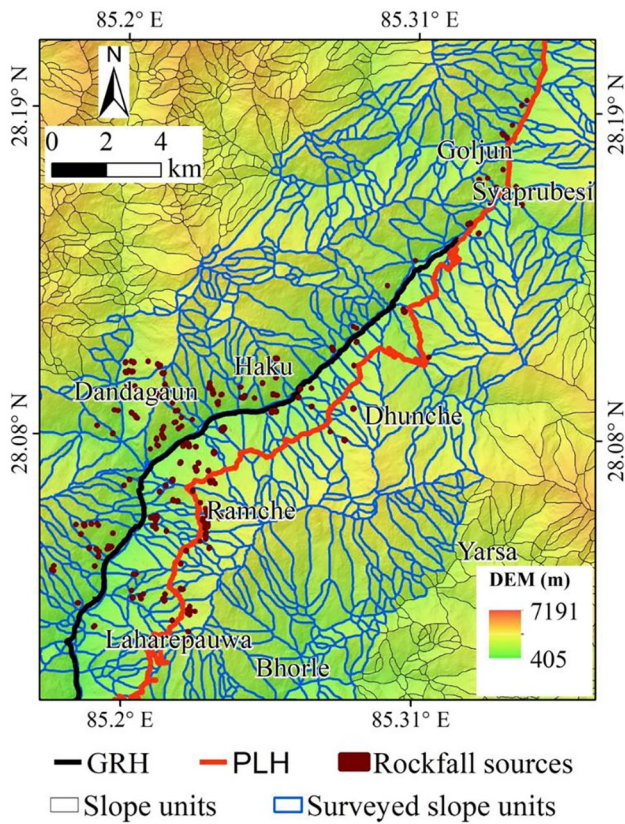


Fig. 4 Map showing rockfall source inventory, slope units in a larger area, and surveyed slope units

rockfall source inventory is available as supplementary material.

- Based on the lithology existing in the study area (Fig. 1), we prepared a table for numerical parameters (dynamic friction, normal restitution, and tangential restitution) required to run STONE (Table 1). We referred to Guzzetti et al. (2004) and Alvioli et al. (2021) to infer the values of numerical parameters from lithology since no such tables are available in the literature for our study area.

Assessment of rockfall sources

The most relevant input of the model STONE is a raster map describing the location of rockfall sources. A typical method to select rockfall source areas (Guzzetti et al. 2003; Losasso et al. 2017; Khatiwada and Dahal 2020; Matas et al. 2017) is to use a slope threshold, meaning that grid cells with a slope above the threshold are considered a rockfall source area.

In this work, we prepared a map of potential rockfall sources based on three geomorphometric parameters: slope angle, relief, and VRM. More specifically, we expand the approach used by Alvioli et al. (2021), who used slope angle distributions to define a probability of rockfalls triggering as a function of the local slope. Here, we use local relief and vector ruggedness measures as well, a similar approach to that already explored by Alvioli et al. (2022b) in a small area in Italy. Unlike Alvioli et al. (2022b), we do not assign a probabilistic meaning to sources, here. Topographic relief is also a predominant factor for rockfall movements (Loye et al. 2009; Kuehnert et al. 2020). Topography’s surface roughness is another geomorphometric factor influencing the rockfall process and its behavior (Wang and Lee 2010; Brožová et al. 2021). Vector ruggedness measure is considered a high-performing algorithm to categorize surface roughness, and it has been used for improving natural hazard modeling (Brožová et al. 2021).

The goal is to choose slope, relief, and VRM joint threshold values above which the probability of having a rockfall source (i.e., a grid cell from which STONE simulates a three-dimensional rockfall trajectory across the underlying topography) is substantially large. To this end, we performed the following steps:

1. We considered 243 field-mapped polygons as a representative sample of rockfall sources in the study area.
2. For each source polygon, we calculated the distribution of slope, relief, and VRM within the polygons. Distributions (normalized histograms) were limited within the whole SU containing the mapped source polygon/

Fig. 5 Rockfalls identified during the field along the Dhunche-Syaprubesi highway. The red polygons are potential rockfall sources, and the blue polygon shows rock blocks that fell off the slope



Table 1 Values of three numerical parameters, used in STONE, for the lithology present in the field (cf. Fig. 1) are assigned referring to Guzzetti et al. (2004) and Alvioli et al. (2021) and geological formation available in Stocklin and Bhattacharai (1977), Stocklin (1980), and DMG (2011)

Rock formation	Lithology noted in the field	Dynamic friction	Normal restitution	Tangential restitution
Q	Recent deposits (alluvial and colluvial deposits)	0.80	15	40
Lk	Limestones, dolomites with intercalation of shales	0.35	60	70
Sy	Slightly weathered quartzites in most of the area, calcareous quartzites	0.35	60	70
Sg	Quartzite in most of the area and a fair presence of limestones	0.40	55	65
Gl	Slates, dolomites	0.35	60	70
Gp	Slates, dolomites, limestones	0.35	60	70
Nd	Quartzites	0.30	65	75
St	Phyllites and quartzites	0.30	65	75
Ul	Schists	0.35	60	70
Hm	Mostly quartzites and schists at some places	0.35	60	70

polygons (cf. the “[Generalization of potential rockfall sources](#)” section).

- As slope, relief, and VMR depend on the size of the calculation neighborhood, we repeated the above step for seven moving window sizes, namely, 3, 5, 7, 9, 15, 21, and 31 grid cells (Hodgson 1998; Turner et al. 2011; Ali et al. 2021). Calculations with several window sizes allow us to find the best scale for the process in relation to the resolution of the DEM (Pain 2005). Slope maps were prepared using *r.param.scale*, relief using *r.neighbors*, and VRM using *r.vector.ruggedness* in GRASS GIS (GRASS Development Team 2017).
- Selection of the window size, which best represents the rockfall source distribution and suitable thresholds of slope, relief, and VRM. Thresholds stem from the analysis of the ratio of the distributions within the mapped polygons, divided by the distributions within the whole slope unit, for each histogram bin and for each unit.

The joint values of the thresholds allow us to obtain the final source map by the intersection of the three conditions on slope, relief, and VRM in GIS. The final map results from extrapolation (generalization) outside the surveyed SUs, assuming that similar conditions would trigger rockfalls in neighboring areas. This ensures that we include potential sources in unsurveyed locations or locations where rockfall did not occur yet but are still prone to fall.

Physically based rockfall susceptibility

The model STONE simulates geometrical trajectories followed by blocks falling independently (i.e., rock avalanches and similar phenomena are not included) under the action of gravity, within the constraints of the digital topography. The main inputs of STONE are (i) a raster map of sources, the generalized rockfall source developed

here in the “[Assessment of rockfall sources](#)” section, (ii) numerical parameters, specific to the lithology of the area (dynamic friction, normal restitution, and tangential restitution), and (iii) DEM covering the area of interest. All these maps are prepared in a grid format, with the exact resolution as the DEM.

STONE calculates three main outputs: (i) count of the number of rockfall trajectories crossing each pixel, (ii) maximum height of trajectories with respect to local elevation, and (iii) maximum velocity of the boulders crossing each cell. We only considered output (i) which we interpret as the spatial likelihood of a grid cell being hit by a rockfall, and thus considered as the rockfall susceptibility in the study area. We used natural breaks to classify the counter map into a rockfall susceptibility index (RSI) in five classes: larger index values indicate high susceptibility. We calculated RSI for the whole rockfall source generalized area.

Comparison and validation of results

Validation of the generalized source map is performed by calculating some measure of the overlap between the map and ground check (here, sources mapped in the field) or an independent inventory (e.g., Alvioli et al. (2021) used a national inventory). Here, the rockfall sources mapped in the field cover much smaller areas than the results obtained from generalization. Hence, a direct comparison would be biased. Therefore, we calculated the percentage of pixels of the field-mapped sources that exactly overlapped with the ones obtained from the generalization. For the runout obtained from STONE, we verified the results in the field, wherever accessible, and used available satellite images (SPOT 6, 7) (cf. the “[STONE outputs and field validation](#)” and “[Discussions](#)” sections).

Results

Generalization of potential rockfall sources

We calculated the distribution of slope values within each rockfall source polygon falling within an SU polygon (i.e., for 243 sources) and the distribution of slope values within the whole SU. We took the ratio of the former over the latter and plotted it in Fig. 6a, for seven moving window sizes. Visual analysis of the ratios reveals that the result for size 3 shows an almost monotonic behavior and a wide range of represented values of slopes. This suggests using window size 3 as the best representation of slope values for rockfall sources in the study area, and selecting the corresponding slope threshold at approximately 50 degrees, an intermediate slope value where the histogram shows the distinctive change. For the relief ratio, we selected window size 15 and thresholds at 290 m (Fig. 6b). We chose window size 7 for VRM and thresholds 0.04 (Fig. 6c). We used these thresholds for slope, relief, and VRM to the whole study area (all of the 1537 SUs) and calculated the final rockfall source map, as mentioned in the “Assessment of rockfall sources” section (Fig. 7), to be used as input for STONE.

The total area covered by the potential rockfall source area, obtained from generalization, is 7.3 km², and the area of slope units over which generalization is performed

is 792.6 km². The total number of field-mapped rockfall sources is 2304, out of which 1762 pixels (76.5%) overlapped with generalized sources, which we deem as a satisfactory agreement. An example of the overlap between the field-mapped rockfall source and the generalized rockfall source is given in the supplementary material.

STONE outputs and field validation

Figure 8 shows the RSM prepared using rockfall trajectory counts from each potential source obtained from STONE (cf. the “Physically based rockfall susceptibility” section). Values of RSI=5 indicate very high rockfall susceptibility, and RSI=1 implies very low susceptibility. We divided each highway into 1 km segments and assigned RSI to each segment. The details are in the supplementary material. According to the results, the Galchhi-Rasuwadhi highway is highly susceptible to rockfall, predominantly in Ramche and Dandagaun villages. The same holds true along the Pasang Lhamu highway, especially around the Syprubesi region. We visited the Syprubesi, Dandagaun, and Ramche sites to validate the results.

We compared our results in Ramche and Dandagaun villages with field observations and satellite images. Identifying rockfall sources in a satellite image is not straightforward. From the images, one can distinguish (Fig. 9a) the whole landslide body and must infer the source area to the

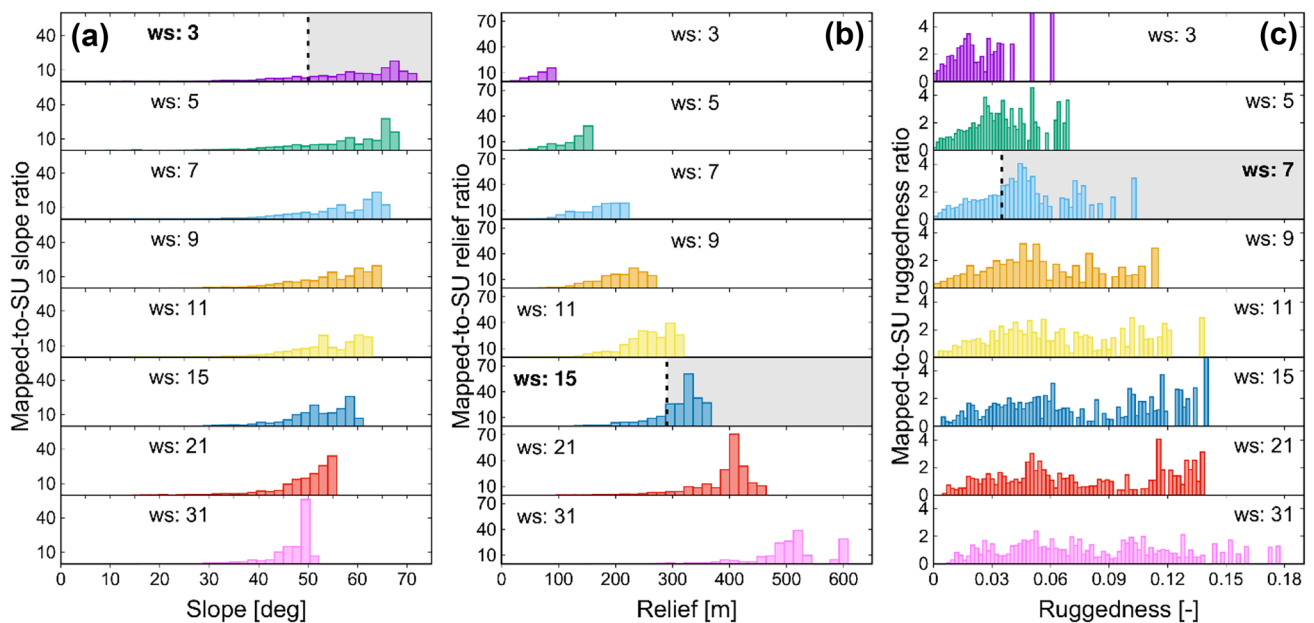


Fig. 6 Histograms illustrating the ratio, for each morphometric parameter, of the distribution of values within mapped source polygons over the distribution within the whole SU containing the mapped polygons: **a**, slope angle; **b**, relief; **c** VRM. For each quan-

tity, we show the ratio for different sizes of the moving window (ws) used to calculate raster maps. The value in bold is the optimal ws; the shaded area shows the values above the threshold value (dashed line)

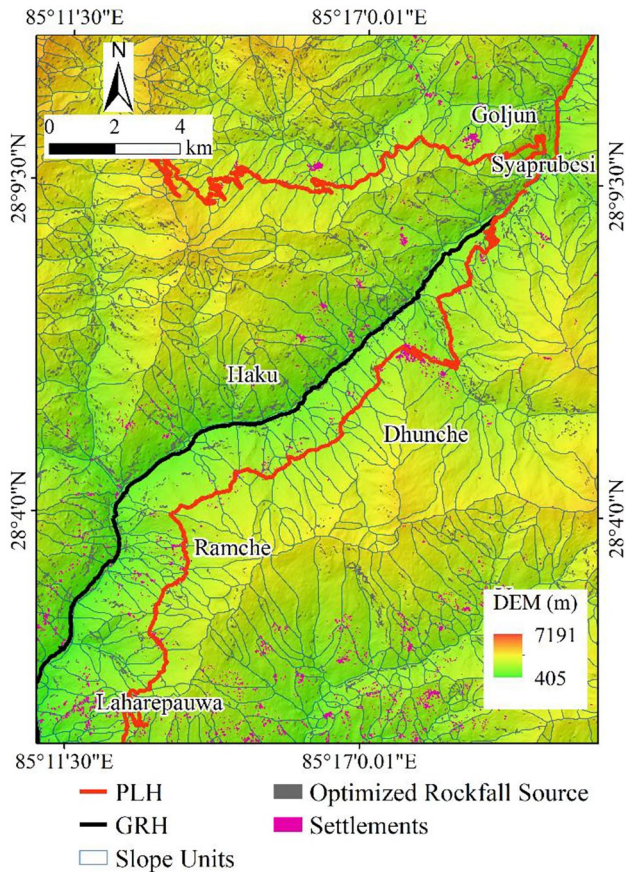


Fig. 7 Map of generalized potential rockfall sources using slope, relief, and VRM thresholds as described in the “Assessment of rockfall sources” section

best of their judgment. Alternatively, one can calculate the subset of the landslide body with higher elevation, for example, with elevation above the 90th percentile of the distribution of elevation inside the polygon. The field investigation in the Ramche area (Fig. 9b) overlaps with the rockfall susceptibility results presented here. In Fig. 9a, the RSI at and around areas 1 and 2 ranges from medium–high. The satellite image in Fig. 9b shows the corresponding location of areas 1 and 2, where the potential rockfall sources and runouts are present. The road section along the slope in Fig. 9a looks highly susceptible to rockfall (and other types of landslides). For the rockfall source area and runouts (Fig. 10) that were difficult to access via roadways, we observed rockfalls from far sight and checked them on Google Earth™. Multiple landslides and rockfalls were seen in this region, with many potential rockfall sources. The degree of weathering was moderate to high in the slope along the roads, as seen in Fig. 10, which indicates a high chance of rockfalls in the future as well.

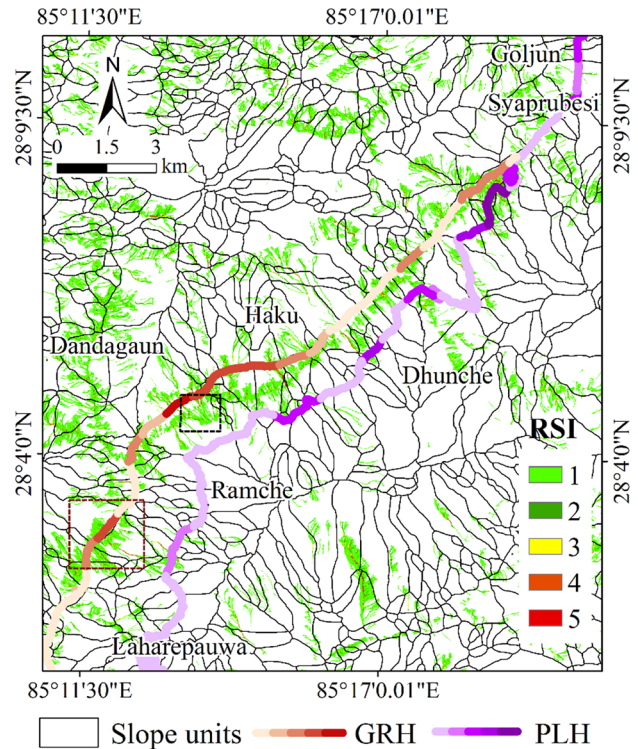


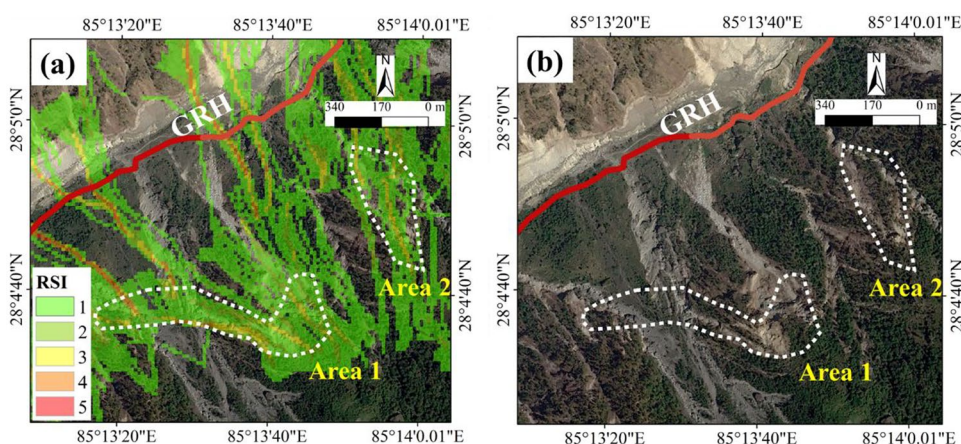
Fig. 8 Rockfall susceptibility map (RSM) of the study area. The highways are divided into 1 km segments each. Values of RSI are classified from 1 (light green, low susceptibility) to 5 (red, high susceptibility). Segments of the roads are classified into five categories as well. GRH and PLH are colorized with red and purple color ramps, respectively, where darker colors correspond to high susceptibility. The black dotted rectangle corresponds to Fig. 9, and the brown dotted rectangle corresponds to Fig. 10

Discussions

Corresponding to the methods and result sections, we discuss generating rockfall source maps based on morphometric thresholds, selection of suitable window sizes for each morphometric parameter, rockfall susceptibility mapping, and its significance for road hazard safety in the Himalayas.

The geology of the study area is dominated by metasedimentary rocks (cf. the “Study area” section) that belong to the Lesser Himalayan Zone and the Higher Himalayan Zone (Stocklin 1980; Dhital 2015), which implies the presence of medium to high-grade metamorphic and high-strength sedimentary rocks. This geological composition contributes to this region’s steep slope topography, resulting in a higher rockfall initiation threshold of slope angles. The complex topography is the main challenge to conducting detailed field-based susceptibility studies. Therefore, our aim in this paper is to implement the data-driven approach to generate a potential rockfall source map.

Fig. 9 **a** Rockfall susceptibility index along a Galchhi-Rasuwgadhi road near Ramche village (in red). The satellite image in the background of **a** is a SPOT 7 from May 03, 2015. **b** Satellite imagery (SPOT 7, May 03, 2015) shows landslide occurrences on the slopes. The red polygon shows mapped rockfall blocks corresponding to two areas in Fig. 11a



The potential rockfall source areas obtained using thresholds for three geomorphometric parameters (slope, window size 3×3 ; relief, size 15×15 ; VRM, size 7×7) presented the best representative distribution of rockfalls (cf. the “Generalization of potential rockfall sources” section). For the other window sizes, the distribution of the parameters was not representative enough. For example, in our study, we argue that the window size of 3×3 and threshold of 50° for slope best represent the field situation. This overlaps with the results from field investigation because, in most of the slopes, rockfall initiation ranges from 50 to 70° . Therefore, selecting window size and thresholds is a significant step, as we can see that the optimal size for each parameter is different, and they strongly affect the results. The results for relief

(size 15×15) and VRM (size 7×7) reflect how the choice of window size can affect the nature of DEM derivatives and, ultimately, susceptibility models.

Our study is a step forward in building realistic rockfall hazard maps, useful for land use planning and, ultimately, rockfall risk reduction and management. Using STONE to prepare RSMs provides a general perspective and understanding of rockfall trajectory distributions along road networks. One of the main advantages of using STONE while conducting the rockfall susceptibility assessment in linear infrastructure such as roads is that it can point to specific places where the route can potentially be interrupted. Henceforth, relevant authorities can conduct a detailed investigation of specific road segments to design rockfall

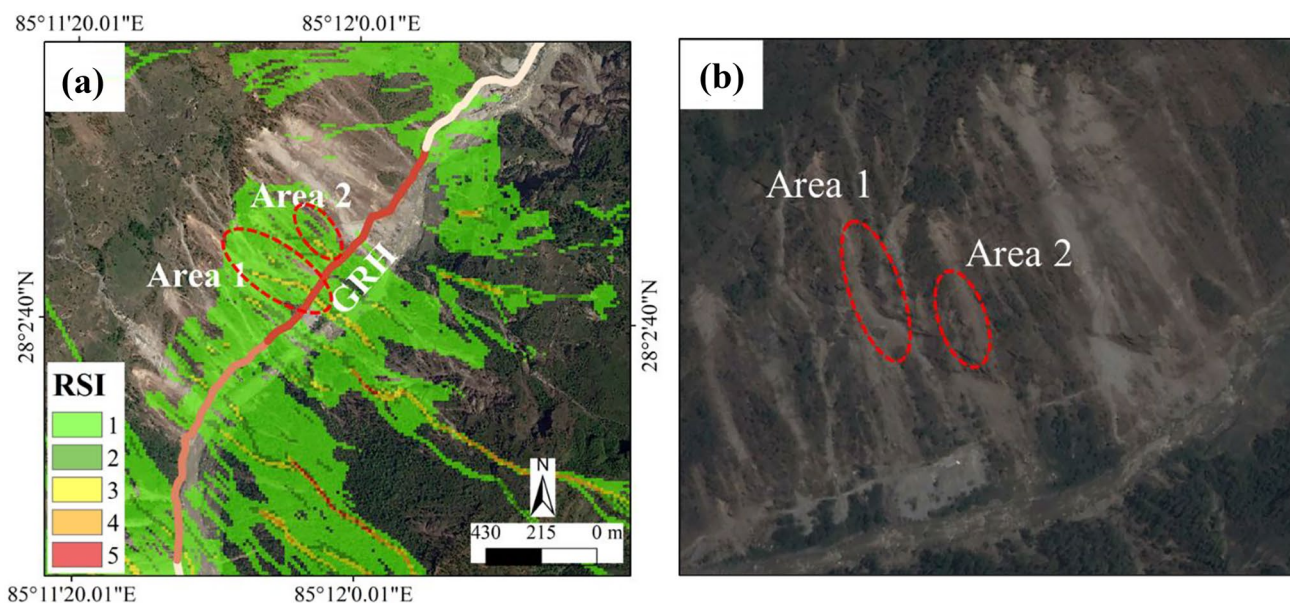
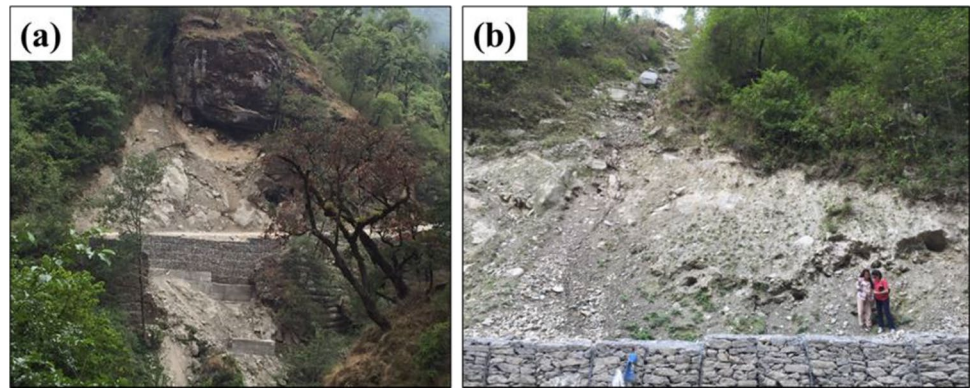


Fig. 10 **a** Rockfall susceptibility index along a Galchhi-Rasuwgadhi road at Deurali Danda near Dandagan village (in ramp of red). The satellite image in the background of **a** is a SPOT 7 from May 03, 2015.

b Google Earth image (May 03, 2015) showing landslide occurrences on the slopes. The red polygon shows the rockfall source area corresponding to two areas in Fig. 10a

Fig. 11 Potential rockfall zones (a 28°6′.8″ N, 85°18′39.6″ E; b 28°6′32.4″ N, 85°18′43.2″ E) along Dhunche–Syprubesi road with gabion walls as the safety measures, which are not sufficient



countermeasures and more sustainable road maintenance. The rockfall source inventory published along with this article as supplementary material may be helpful, along with the results of this study, for independent assessment of rockfall susceptibility and hazards in this area and to set up countermeasures.

Along with the seismicity of Central Nepal Himalayas and geomorphometric factors contributing to landslides (Nugraha et al. 2015; Pokharel et al. 2020) like rockfalls (Loye et al. 2009; Alvioli et al. 2020), the lack of engineering standards in road construction in Central Nepal has triggered these phenomena (Lennartz 2013; McAdoo et al. 2018). Our field visits and local reports suggest that most of the road network lacks necessary rockfall preventive measures, imposing a significant risk to people using these roads (Fig. 11).

Frequent disturbances in road functioning are created by the failure of these safety measures and the new construction of similar structures, which eventually impact the socioeconomic aspects of society and the country in the long run. The RSM we prepared for this region could be a reference for the decision makers to prioritize sites for detailed rockfall hazard assessment to design rockfall safety measures. For example, the areas with RSI 5 and 4, which covers about 39% of GRH highway and 6–8% of PLH, would be the highest priority of time, energy, and financial resources for detailed rockfall studies and mitigation measures.

Conclusions

Active tectonics and high precipitation in Central Nepal Belts cause frequent rockfalls. This has caused severe impacts on communities and infrastructure, especially road networks. Rockfall susceptibility, hazard, and risk along roads are intertwined with environmental issues and sustainable road development. As the first step of rockfall hazard and risk assessment, we generated an RSM in some sections of two major highways, PLH and GRH, in Central Nepal by using a physically based model called STONE.

Owing to the unavailability of rockfall inventories and difficulty in accessing most rockfall-prone sites, we mapped rockfall sources in some selected locations in the field. We prepared a map of potential rockfall sources, based on morphometric analysis of slope, relief, and VRM. We considered histograms, representing the ratio of rockfalls and each morphometric parameter within a SU, in moving windows of seven different sizes and selected a joint (slope, relief, and VRM) rockfall threshold, which is the novelty of our work. We chose the optimal size for each variable, in which suitable thresholds were chosen. The rockfall trajectories (runout) obtained from STONE are an effective tool for selecting target areas where detailed assessments are required. Our field study shows that the highways running through Dandagaun, Ramche, and Syprubesi have high rockfall susceptibility. However, no proper rockfall protection strategies were adopted in these areas, which has affected road management and degraded the surrounding environment. A classified susceptibility index presented in this study would help to prioritize the sections of linear infrastructure, such as a road section that requires detailed rockfall studies and safety measures.

The lack of rockfall data at a nationwide or even district level, which is often the case in this study area, makes validating the work very challenging. Hence, to check if the rockfall map generated matched with real field or not, we relied on the rockfall sources inventory prepared by B.P and T.B and related field reports. Since no similar initiatives have been adopted in this region, our work provides a perspective to preliminary rockfall susceptibility assessment, which is an input to the detailed rockfall hazard and risk assessment as well as sustainable land use planning.

The use of a high-resolution DEM in specific portions of the study area, and a detailed lithological map, would improve the selection of the rockfall source areas. Knowledge of block sizes, detailed geomorphological settings, and possibly the inclusion of specific triggers for rockfalls (for example, a seismic trigger, as in Alvioli et al. (2022c) would help in the quantitative estimation of rockfall hazards. On

the other hand, including the accurate location of infrastructure such as bridges and tunnels, as well as knowledge of details on transit, would allow accurate risk assessment.

Supplementary Information The online version contains supplementary material available at <https://doi.org/10.1007/s10064-023-03174-8>.

Acknowledgements B.P. thanks the Australian Government Research Training Program at the University of New South Wales, Australia, for sponsoring her PhD research, the HPC-Europa3 consortium for a mobility grant and use of HPC facilities, and CNR IRPI (Perugia, Italy) for hospitality. B.P. thanks the Humanitarian Engineering Program, Faculty of Engineering, UNSW Sydney, for providing a research support grant.

Funding Open Access funding enabled and organized by CAUL and its Member Institutions.

Data availability The supplementary material contains vector maps (in GeoPackage format, EPSG:32645) of rockfall sources (polygons) and RSI for both highway paths (line segments) investigated in this work. Any additional data is available upon request.

Declarations

Conflict of interest The authors declare no competing interests.

Open Access This article is licensed under a Creative Commons Attribution 4.0 International License, which permits use, sharing, adaptation, distribution and reproduction in any medium or format, as long as you give appropriate credit to the original author(s) and the source, provide a link to the Creative Commons licence, and indicate if changes were made. The images or other third party material in this article are included in the article's Creative Commons licence, unless indicated otherwise in a credit line to the material. If material is not included in the article's Creative Commons licence and your intended use is not permitted by statutory regulation or exceeds the permitted use, you will need to obtain permission directly from the copyright holder. To view a copy of this licence, visit <http://creativecommons.org/licenses/by/4.0/>.

References

- Ali SD, Fithria A, Rahmadi A, Rezekiah AA (2021) On finding optimal speckle filtering for extraction of vegetation biophysical information using Sentinel-1 SAR imagery. In: Wicaksono P, Wibowo SB (eds) Seventh Geoinformation Science Symposium 2021. SPIE, p 5. <https://doi.org/10.1117/12.2615135>
- Alvioli M, Falcone G, Mendicelli A et al (2023) Seismically induced rockfall hazard from a physically based model and ground motion scenarios in Italy. *Geomorphology* 429:108652. <https://doi.org/10.1016/j.geomorph.2023.108652>
- Alvioli M, Marchesini I, Pokharel B et al (2022a) Geomorphological slope units of the Himalayas. *Journal of Maps* 1–14. <https://doi.org/10.1080/17445647.2022.2052768>
- Alvioli M, Guzzetti F, Marchesini I (2020) Parameter-free delineation of slope units and terrain subdivision of Italy. *Geomorphology* 358:107124. <https://doi.org/10.1016/j.geomorph.2020.107124>
- Alvioli M, Marchesini I, Reichenbach P et al (2016) Automatic delineation of geomorphological slope units with r.slopeunits v1.0 and their optimization for landslide susceptibility modeling. *Geosci Model De* 9:3975–3991. <https://doi.org/10.5194/gmd-9-3975-2016>
- Alvioli M, Santangelo M, Fiorucci F et al (2021) Rockfall susceptibility and network-ranked susceptibility along the Italian railway. *Eng Geol* 293:106301. <https://doi.org/10.1016/j.enggeo.2021.106301>
- Alvioli M, De Matteo A, Castaldo R et al (2022b) Three-dimensional simulations of rockfalls in Ischia, Southern Italy, and preliminary susceptibility zonation. *Geomat Nat Haz Risk* 13(1):2712–2736. <https://doi.org/10.1080/19475705.2022.2131472>
- Alvioli M, Falcone G, Mendicelli A et al (2022c) Seismically induced rockfall hazard from ground motion scenarios in Italy. Preprint: <https://doi.org/10.2139/ssrn.4156514>
- Amatya P, Kirschbaum D, Stanley T, Tanyas H (2021) Landslide mapping using object-based image analysis and open source tools. *Eng Geol* 282:106000. <https://doi.org/10.1016/j.enggeo.2021.106000>
- Antoniu AA, Lekkas E (2010) Rockfall susceptibility map for Athinios port, Santorini Island, Greece. *Geomorphology* 118:152–166. <https://doi.org/10.1016/j.geomorph.2009.12.015>
- Bhattarai TN, Dhital MR (2021) Impact of 2015 Gorkha earthquake on Nepal's hydropower projects: a review and lessons learnt. *J Stage* 31:64–72. <https://doi.org/10.11315/jstage.31.64>
- Brožová N, Baggio T, D'agostino V et al (2021) Multiscale analysis of surface roughness for the improvement of natural hazard modelling. *Nat Hazard* 21:3539–3562. <https://doi.org/10.5194/nhess-21-3539-2021>
- Chen C-H, Ke C-C, Wang C-L (2009) A back-propagation network for the assessment of susceptibility to rock slope failure in the eastern portion of the Southern Cross-Island Highway in Taiwan. *Environ Geol* 57:723–733. <https://doi.org/10.1007/s00254-008-1350-9>
- Cignetti M, Godone D, Bertolo D et al (2021) Rockfall susceptibility along the regional road network of Aosta Valley Region (north-western Italy). *J Maps* 17:54–64. <https://doi.org/10.1080/17445647.2020.1850534>
- Collins BD, Jibson RW (2015) Assessment of existing and potential landslide hazards resulting from the April 25, 2015 Gorkha, Nepal earthquake sequence (ver. 1.1, August 2015) U.S. Geological Survey Open-file Report 2015–1142. 50. <https://doi.org/10.3133/ofr20151142>
- Dawadi B, Shrestha A, Acharya RH et al (2022) Impact of climate change on agricultural production: a case of Rasuwa District, Nepal. *Regional Sustainability* 3:122–132. <https://doi.org/10.1016/j.regsus.2022.07.002>
- Dhital MR (2015) Geology of the Nepal Himalaya: regional perspective of the classic collided orogen (Regional Geology Reviews). Springer International Publishing, USA, p 498. <https://doi.org/10.1007/978-3-319-02496-7>
- DMG (2011) Geological map published by Department of Mines and Geology (DMG), Accessed 12 September 2022, <https://www.dmgnepal.gov.np/>
- Domènech G, Alvioli M, Corominas J (2020) Preparing first-time slope failures hazard maps: from pixel-based to slope unit-based. *Landslides* 17:249–265. <https://doi.org/10.1007/s10346-019-01279-4>
- GRASS Development Team (2017) Geographic Resources Analysis Support System (GRASS) Software, Version 7.2. Open Source Geospatial Foundation. Electronic document. Accessed 12 September 2022. <http://grass.osgeo.org>
- Guillard C, Zezere J (2012) Landslide susceptibility assessment and validation in the framework of municipal planning in Portugal: the case of Loures municipality. *Environ Manage* 50:721–735. <https://doi.org/10.1007/s00267-012-9921-7>
- Guzzetti F (2000) Landslide fatalities and the evaluation of landslide risk in Italy. *Eng Geol* 58:89–107. [https://doi.org/10.1016/S0013-7952\(00\)00047-8](https://doi.org/10.1016/S0013-7952(00)00047-8)
- Guzzetti F, Crosta G, Detti R, Agliardi F (2002) STONE: a computer program for the three-dimensional simulation of rock-falls. *Comput Geosci* 28:1079–1093. [https://doi.org/10.1016/S0098-3004\(02\)00025-0](https://doi.org/10.1016/S0098-3004(02)00025-0)

- Guzzetti F, Reichenbach P, Ghigi S (2004) Rockfall hazard and risk assessment along a transportation corridor in the Nera valley, central Italy. *Environ Manage* 34:191–208. <https://doi.org/10.1007/s00267-003-0021-6>
- Guzzetti F, Reichenbach P, Wieczorek GF (2003) Rockfall hazard and risk assessment in the Yosemite Valley, California, USA. *Nat Hazards Earth Syst Sci* 3:491–503. <https://doi.org/10.5194/nhess-3-491-2003>
- Guzzetti F, Mondini AC, Cardinali M, Fiorucci F, Santangelo M, Chang KT (2012) Landslide inventory maps: new tools for an old problem. *Earth Sci Rev* 112:42–66. <https://doi.org/10.1016/j.earscirev.2012.02.001>
- Hodgson ME (1998) What size window for image classification? A cognitive perspective. *Photogramm Eng Remote Sens* 64:797–807
- Jacobs L, Kervyn M, Reichenbach P, Rossi M, Marchesini I, Alvioli M, Dewitte O (2020) Regional susceptibility assessment with heterogeneous landslide information: slope unit- vs. pixel-based approach. *Geomorphology* 356:107084. <https://doi.org/10.1016/j.geomorph.2020.107084>
- Karlsson CSJ, Kalantari Z, Mörtberg U et al (2017) Natural hazard susceptibility assessment for road planning using spatial multi-criteria analysis. *Environ Manage* 60:823–851. <https://doi.org/10.1007/s00267-017-0912-6>
- Khatiwada D, Dahal RK (2020) Rockfall hazard in the Imja Glacial Lake, eastern Nepal. *Geoenvironmental Disasters* 7:29. <https://doi.org/10.1186/s40677-020-00165-9>
- Kuehnert J, Mangeney A, Capdeville Y et al (2020) Simulation of topography effects on rockfall-generated seismic signals: application to Piton de la Fournaise Volcano. *J Geophys Res Solid Earth* 125. <https://doi.org/10.1029/2020JB019874>
- Lacroix P (2016) Landslides triggered by the Gorkha earthquake in the Langtang valley, volumes and initiation processes. *Earth, Planets and Space* 68. <https://doi.org/10.1186/s40623-016-0423-3>
- Lennartz T (2013) Constructing roads—constructing risks? Settlement decisions in view of landslide risk and economic opportunities in western Nepal. *Mt Res Dev* 33:364–371. <https://doi.org/10.1659/MRD-JOURNAL-D-13-00048.1>
- Lin YP, Chang TK, Wu CF et al (2006) Assessing impacts of typhoons and the Chi-Chi earthquake on Chenyulan watershed landscape pattern in central Taiwan using landscape metrics. *Environ Manage* 38:108–125. <https://doi.org/10.1007/s00267-005-0077-6>
- Loche M, Alvioli M, Marchesini I, Bakka H, Lombardo L (2022) Landslide susceptibility maps of Italy: lesson learnt from dealing with multiple landslide types and the uneven spatial distribution of the national inventory. *Earth Sci Rev* 104125. <https://doi.org/10.1016/j.earscirev.2022.104125>
- Losasso L, Jaboyedoff M, Sdao F (2017) Potential rock fall source areas identification and rock fall propagation in the province of Potenza territory using an empirically distributed approach. *Landslides* 14:1593–1602. <https://doi.org/10.1007/s10346-017-0807-x>
- Loye A, Jaboyedoff M, Pedrazzini A (2009) Identification of potential rockfall source areas at a regional scale using a DEM-based geomorphometric analysis. *Natural Hazards and Earth System Science* 9:1643–1653. <https://doi.org/10.5194/nhess-9-1643-2009>
- Martha TR, Roy P, Mazumdar R et al (2017) Spatial characteristics of landslides triggered by the 2015 Mw 7.8 (Gorkha) and Mw 7.3 (Dolakha) earthquakes in Nepal. *Landslides* 14:697–704. <https://doi.org/10.1007/s10346-016-0763-x>
- Matas G, Lantada N, Corominas J et al (2017) RockGIS: a GIS-based model for the analysis of fragmentation in rockfalls. *Landslides* 14:1565–1578. <https://doi.org/10.1007/s10346-017-0818-7>
- McAdoo BG, Quak M, Gnyawali KR et al (2018) Roads and landslides in Nepal: how development affects environmental risk. *Nat Hazard* 18:3203–3210. <https://doi.org/10.5194/nhess-18-3203-2018>
- Nugraha H, Wacano D, Dipayana GA et al (2015) Geomorphometric characteristics of landslides in the Tinalah Watershed, Menoreh Mountains, Yogyakarta, Indonesia. *Procedia Environ Sci* 28:578–586. <https://doi.org/10.1016/j.proenv.2015.07.068>
- Pain CF (2005) Size does matter: Relationships between image pixel size and landscape process scales. In: MODSIM05 - International Congress of Modelling and Simulation. Modelling and Simulation Society of Australia and New Zealand Inc. Citeseer 1430–1436
- Pradhan SP, Vishal V, Singh TN (2015) Study of slopes along River Teesta in Darjeeling Himalayan region. *Engineering Geology for Society and Territory* -, vol 1. Springer International Publishing, Cham, pp 517–520
- Pokharel B, Althwaynee OF, Aydda A et al (2021a) Spatial clustering and modelling for landslide susceptibility mapping in the north of the Kathmandu Valley, Nepal. *Landslides*. <https://doi.org/10.1007/s10346-020-01558-5>
- Pokharel B, Alvioli M, Lim S (2020) Relevance of morphometric predictors and completeness of inventories in earthquake-induced landslide susceptibility. In: Alvioli M, Marchesini I, Laura M, Peter G (eds) *Proceedings of the Geomorphometry 2020 Conference*, Perugia, Italy, 22–23 June 2020 (online), pp 182–185. https://doi.org/10.30437/GEOMORPHOMETRY2020_49
- Pokharel B, Alvioli M, Lim S (2021b) Assessment of earthquake-induced landslide inventories and susceptibility maps using slope unit-based logistic regression and geospatial statistics. *Sci Rep* 11:21333. <https://doi.org/10.1038/s41598-021-00780-y>
- Pokharel B, Thapa PB (2019) Landslide susceptibility in Rasuwa District of central Nepal after the 2015 Gorkha Earthquake. *Journal of Nepal Geological Society* 59:79–88. <https://doi.org/10.3126/jngs.v59i0.24992>
- Regmi AD, Cui P, Dhital MR, Zou Q (2016a) Environmental Earth Sciences 75:1112. <https://doi.org/10.1007/s12665-016-5905-x>
- Regmi AD, Dhital MR, Qiang ZJ et al (2016b) Landslide susceptibility assessment of the region affected by the 25 April 2015 Gorkha earthquake of Nepal. *J Mt Sci* 13:1941–1957. <https://doi.org/10.1007/s11629-015-3688-2>
- Stocklin J, Bhattacharai KD (1977) Geology of the Kathmandu area and central Mahabharat range, Nepal Himalaya. Report of Department of Mines and Geology/UNDP
- Stocklin J (1980) Geology of Nepal and its regional frame. *J Geol Soc London* 137:1–34. <https://doi.org/10.1144/gsjgs.137.1.0001>
- Toševski A, Pollak D, Perković D (2021) Identification of rockfall source areas using the seed cell concept and bivariate susceptibility modelling. *Bull Eng Geol Env* 80:7551–7576. <https://doi.org/10.1007/s10064-021-02441-w>
- Turner R, Stone C, Kathuria A, Penman T (2011) Towards an operational lidar resource inventory process in Australian softwood plantations. In: *Proceedings of the 34th International Symposium for Remote Sensing of the Environment (ISRSE)*, Sydney, Australia
- Vishal V, Pradhan SP, Singh TN (2015) Analysis of stability of slopes in Himalayan Terrane along national highway: 109, India. *Engineering Geology for Society and Territory* -, vol 1. Springer International Publishing, Cham, pp 511–515
- Vishal V, Siddique T, Purohit R et al (2017) Hazard assessment in rockfall-prone Himalayan slopes along National Highway-58, India: rating and simulation. *Nat Hazards* 85:487–503. <https://doi.org/10.1007/s11069-016-2563-y>
- Wang IT, Lee CY (2010) Influence of slope shape and surface roughness on the moving paths of a single rockfall. *World Acad Sci Eng Technol* 65:122–128. <https://doi.org/10.5281/zenodo.1059437>
- Xu C, Tian Y, Zhou B et al (2017) Landslide damage along Araniko highway and Pasang Lhamu highway and regional assessment of landslide hazard related to the Gorkha, Nepal earthquake of 25 April 2015. *Geoenvironmental Disasters* 4:14. <https://doi.org/10.1186/s40677-017-0078-9>